Materials for Quantum Technology

Absorptive laser threshold magnetometry: combining visible diamond Raman lasers and nitrogen-vacancy centres

Materials for Quantum Technology

PAPER

Absorptive laser threshold magnetometry: combining visible diamond Raman lasers and nitrogen-vacancy centres

Sarath Raman Nair[1,2,*], Lachlan J Rogers[1,2,3], David J Spence[1], Richard P Mildren[1], Fedor Jelezko[4], Andrew D Greentree[5], Thomas Volz[1,2] and Jan Jeske[6]

[1] Department of Physics and Astronomy, Macquarie University, NSW 2109, Australia
[2] ARC Centre of Excellence for Engineered Quantum Systems, Macquarie University, NSW 2109, Australia
[3] School of Mathematical and Physical Sciences, University of Newcastle, NSW 2308, Australia
[4] Institute for Quantum Optics, Ulm University, Albert-Einstein-Allee 11, D-89081, Ulm, Germany
[5] ARC Centre of Excellence for Nanoscale BioPhotonics, School of Science, RMIT University, Melbourne, VIC 3001, Australia
[6] Fraunhofer Institut für Angewandte Festkörperphysik IAF, Tullastrasse 72, 79108 Freiburg, Germany
[*] Author to whom any correspondence should be addressed.

E-mail: sarath.raman-nair@mq.edu.au

Keywords: nitrogen-vacancy centres, laser threshold magnetometry, diamond Raman laser, diamond colour centres, optical micro-cavity

OPEN ACCESS

RECEIVED
26 January 2021

REVISED
12 April 2021

ACCEPTED FOR PUBLICATION
29 April 2021

PUBLISHED
21 June 2021

Abstract

We propose a high-sensitivity magnetometry scheme based on a diamond Raman laser with visible pump absorption by an ensemble of coherently microwave driven negatively charged nitrogen-vacancy centres (NV^-) in the same diamond crystal. The NV^- centres' absorption and emission are spin-dependent. We show how the varying absorption of the NV^- centres changes the Raman laser output. A shift in the diamond Raman laser threshold and output occurs with the external magnetic field and microwave driving. We develop a theoretical framework with steady-state solutions to describe the effects of coherently driven NV^- centres including the charge state switching between NV^- and its neutral charge state NV^0 in a diamond Raman laser. We discuss that such a laser working at the threshold can be employed for magnetic field sensing. In contrast to previous studies on NV^- magnetometry with visible laser absorption, the laser threshold magnetometry method is expected to have low technical noise, due to low background light in the measurement signal. For magnetic-field sensing, we project a shot-noise limited DC sensitivity of a few pT $/\sqrt{\text{Hz}}$ in a well-calibrated cavity with realistic parameters. This sensor employs the broad visible absorption of NV^- centres and unlike previous laser threshold magnetometry proposals it does not rely on active NV^- centre lasing or an infrared laser medium at the specific wavelength of the NV^- centre's infrared absorption line.

1. Introduction

Negatively charged nitrogen-vacancy (NV^-) centres in diamond are being widely explored as quantum sensors for magnetic fields [1–4], electric fields [5, 6], pressure [7] and temperature [3, 8]. They are also promising candidates for qubits [9], fluorescent biomarkers [10–12], nanoscale [13, 14] and microscale [15, 16] magnetic field mapping, decoherence microscopy [17–19], nanoscale nuclear magnetic resonance [20], optical trapping [21], laser-cooling [22] and gyroscopes [23]. For sensing, NV^- centres have the potential to achieve room-temperature operation enabling sensing without the need for insulation barriers between the sensor and sources such as biological tissue. Such complications are needed in other high-sensitivity technologies such as cryogenic superconducting quantum interference devices and vapour cell magnetometers.

Laser threshold magnetometry (LTM) [24–28] is a new concept of magnetic field sensing that harnesses the non-linearity of a laser cavity to strongly improve sensitivity to small magnetic field changes. Microwave (MW) driven negatively charged NV^- centres were proposed [24] as an active laser gain medium, such that the laser threshold shifts with the external magnetic field. Small magnetic field changes then result in strong changes of the laser output power, leading (theoretically) to a huge improvement of the shot-noise limited DC sensitivities potentially down to the order of fT $/\sqrt{\text{Hz}}$ for a crystal sensing volume of 1 mm^3. Such sensitivity

range would be several orders of magnitude better than even the state of the art AC magnetometry with NV^- centres [29]. Although the stimulated emission of NV^- centres without an external cavity [25] and also the amplification of an external continuous-wave (CW) laser transmission due to the optical gain by the stimulated emission of NV^- centres in an optical cavity at steady state [26] have been shown in experiments, the challenge of achieving a CW NV^- lasing required for the LTM is still outstanding to the best of our knowledge. A variation has been proposed [28], which does not require active NV^- lasing, but instead the idea is to use infrared (IR) singlet transition of the NV^- centre (1042 nm) as a variable absorber inside the cavity of another IR active gain medium, thus can shift the IR laser threshold with the external magnetic field. This study predicted a theoretical shot-noise DC sensitivity around 700 fT $/\sqrt{\text{Hz}}$. However, for this idea to work an intracavity IR laser medium needs to be matched with the relatively narrow absorption line upon which sensing is then based. Moreover, the IR wavelength absorption by NV^- centre is weak compared to visible wavelength absorption. Both are promising and recent concepts, which have not yet been experimentally realised.

Here we propose a new absorptive LTM approach using the broad visible absorption spectrum of the NV^- centre as a magnetically controlled absorber [30, 31] of the pump wavelength inside the cavity of a diamond Raman laser. Raman lasers rely on amplification of a cavity Stokes field through stimulated scattering of a pump by zone-centre phonons [32]. Hence the threshold of a diamond Raman laser is influenced by the intensity of the pump field or the cavity quality factor at the Stokes frequency, and is dependent on absorption by impurities. As a result, traditional diamond Raman lasers require highly perfect diamond crystals, and so defect centres are seen as sources of scattering and loss. Investigating the effects of NV^- centres in diamond Raman lasing [33–35] is an interesting new perspective for sensing using the concept of LTM. Since the absorption of the pump by NV^- centres changes the threshold of the Raman laser, the Raman laser threshold in turn changes with external magnetic field. We provide the first investigation of the effects of absorption by NV^- centres on diamond Raman lasers and our study shows that NV^- centres in diamond Raman crystal can instead be a resource for sensing based on the spin-dependent ground state population of these centres and its variation with magnetic field.

Compared to most NV^- magnetometry schemes our approach is based on the existing absorption-based magnetometry, which relies on the absorption of a visible external laser transmitting through the diamond with NV^- centres [30, 31]. This absorption-based scheme has opposite behaviour of bright and dark states: upon transition to the 'darker' $m_s = \pm 1$ state the relatively long-lived singlet state is populated and thus the ground state population reduced. This results in reduced NV^- absorption and thus stronger Raman laser output in our case. Thus the commonly 'darker' $m_s = \pm 1$ state, which shows less fluorescence, actually leads to higher signal output than the $m_s = 0$ spin state in the absorption-based scheme.

In contrast to the existing visible absorption-based magnetometry [30, 31], in which change in the laser transmission with magnetic field is of interest, our method working at a laser threshold has the advantage of significant reduction of background light, with which a low technical noise while measurements is expected. The present concept allows the combination of NV^- centres with an established active laser system [34–36], which is also based on diamond crystals. Comparing with two separate media in the IR LTM proposed in [28], the absorption and light generation in our present study can be realised in a single crystal. The properties of the Raman gain mechanism offer a wide diversity of options for implementing the Raman laser: operation is compatible with almost any wavelength throughout the wide transmission band of diamond, overlapping with the broad visible absorption band, IR absorption, and both near IR as well as IR emission of the NV^- centre. The broad visible wavelength absorption, which is the focus in the present study, allows for multiple laser wavelengths in the visible range and improves robustness of the sensing concept against wavelength fluctuations relative to the narrow absorption of the IR transition. Laser operation is also compatible across a wide range of temporal regimes (continuous to ultrafast pulses) [37–41]. Designs have been demonstrated in several physical formats including high-power free-space designs [35], efficient monolithic devices [42] and miniature on-chip devices with low threshold (<80 mW [43]). Hence magnetic field sensors based on Raman lasing may take a variety of forms and operate across a wide range of scales.

This article is organized in three sections. In section 1, we model a CW diamond Raman laser in a Fabry–Perot cavity with intra-cavity absorption by MW driven negatively-charged NV^- centres in the same diamond crystal. We show numerical results of the Raman laser output in the presence of an external magnetic field and its sensitivity in section 2. In section 3, we conclude by discussing the implications of the results in actual experimental scenarios.

2. Model

We model CW diamond Raman laser system that works at ambient conditions, considering MW driven NV^- centres in the same diamond crystal as intra-cavity absorbers. The visible absorption band of the NV^- centres,

more precisely the diamond crystal containing NV^- centres roughly spans from 450 nm to 700 nm [1, 22, 44, 45]. The zero-phonon line (ZPL) of the NV^- centre is at 637 nm, which corresponds to around 471 THz. Due to the characteristic diamond Raman shift, the Raman laser frequency is 40 THz lower than that of the pump light frequency, i.e. the respective wavelength is higher. NV^- centres can in principle absorb both pump and Raman wavelengths, if both these wavelengths fall into the absorption band of the centres. Magnetic-field detection using the absorption by NV^- centres is possible only if there is a steady-state population in the NV^- centres' ground state available for spin manipulation. The intense intra-cavity field of the Raman wavelength will quickly saturate the NV^-s to its excited state or singlet states, thus removing any potential for the variation of ground state population and absorption. Furthermore bistable behaviour [46–48] above threshold can occur, since NV^- centres are saturable absorbers. Hence we consider the desired operating condition with pump wavelength in the absorption spectrum of the NV^- centres, i.e. below the ZPL, and a Raman wavelength outside that absorption spectrum, i.e. above the ZPL.

For this study, we consider that the pump wavelength (λ_p) is 620 nm (around 484 THz), which is at the upper end of the NV^- absorption spectrum, and thus the corresponding Raman wavelength (λ_r) is around 676 nm (around 444 THz). Though the tail of the experimental absorption band of diamond containing NV^- centres includes the Raman wavelength around 676 nm [22, 45], we neglect the absorption of this wavelength by the NV^- centres for two reasons. First, the Raman laser photons are not expected to excite NV^- centres from their ground state to the excited state, since these photons are red-detuned by around 27 THz with respect to the ZPL of the NV^- centre. Second, we do not expect a significant steady-state population to occupy the phonon levels of the NV^- ground state, as they have extremely short lifetime on the order of picoseconds [24]. Hence, we consider that the NV^- centres absorb only the pump wavelength at 620 nm.

The steady-state population in the NV^- centres' ground state can also be affected due to the light-induced charge state switching of between NV^- centres and their neutral charge state, denoted as NV^0 centres [26, 44, 49–51]. Thus we consider in our model that the NV^- centre in the diamond can have two charge states NV^- and NV^0 due to the light-induced charge state switching. For the rest of this study we denote the light induced charge state switching from NV^- to NV^0 as the ionization process and the reverse switching from NV^0 to NV^- as the recombination process. The charge state switching due to the wavelengths that we consider in this study is expected to be a two photon process [26, 44, 49, 51]. That is, the charge state switching happens from the excited state after the respective centre gets excited by the light. The minimum photon energy required for the ionization process, i.e. for removing an electron from the excited state of the NV^- to the valence band, which is located around 0.6 eV [49] above it, is expected to be around 1.56 eV [52]. Similarly, for the recombination process the minimum photon energy required to extract an electron from the P1 (nitrogen atom) centres, which are expected to be one of the main charge donors is 1.7 eV [53–56]. Since both the λ_p (around 2 eV) and λ_r (around 1.84 eV) have the photon energy higher than these specified energies, they can in principle induce charge state switching from the excited states of NV^- and NV^0. However, both these wavelengths are not expected to excite NV^0 since λ_p and λ_r are around 38 THz and 78 THz respectively red-detuned with respect ZPL of the NV^0 at 575 nm [1]. In order to excite NV^0 charge state, we require an additional laser whose wavelength is $\leqslant$575 nm. In this study we consider continuous pumping of an additional CW green laser (λ_{gr}) close to 532 nm through the cavity to help re-pumping the NV^0 back to its negative charge state.

We obtain a steady-state solution to the CW diamond Raman laser system incorporating MW driven NV^- centres at ambient conditions in two steps. Firstly, we model NV^- centres coherently driven by MW including charge state switching to NV^0 as the absorbers, in section 2.1. Secondly, we model the diamond Raman laser including the absorbers to get a pump-laser output relation in section 2.2). The schematic of our model is shown in figure 1.

2.1. MW driven NV^- centres as the absorbers in the crystal

We assume all the NV^- (and NV^0) centres in the crystal are non-interacting and identical absorbers. NV^- (and NV^0) centres are typically oriented along four different crystal directions. For simplicity, we work with only one orientation. This can be achieved in a crystal produced with preferential orientation [57]. At ambient conditions, each NV^- centre in the ensemble can be represented as a seven-level system as shown in figure 1 [58]. The two spin $m_s = \pm 1$ levels considered, can be separated by lifting the degeneracy using Zeeman effect by applying a background magnetic field along the quantization axis [1, 58]. Levels $|1\rangle$, $|2\rangle$, and $|3\rangle$ represent $m_s = 0$, $m_s = -1$, and $m_s = +1$ levels of the ground state respectively, levels $|4\rangle$, $|5\rangle$, and $|6\rangle$ represent the $m_s = 0$, $m_s = -1$, and $m_s = +1$ levels of the excited state. We represent the singlet states as a single level. Furthermore, we also consider NV^0 centre as a two level system for including the effect of light induced charge state switching of NV^- and NV^0 centre [26, 28, 51]. The ground and excited states of the NV^0 are represented as $|8\rangle$ and $|9\rangle$ respectively.

The ground state levels $|1\rangle$ and $|2\rangle$ are resonantly driven by MW with a driving (Rabi) frequency Ω_d. We assume that the incoherent optical pumping of the NV centres with λ_p and λ_{gr} excites the NV centre from

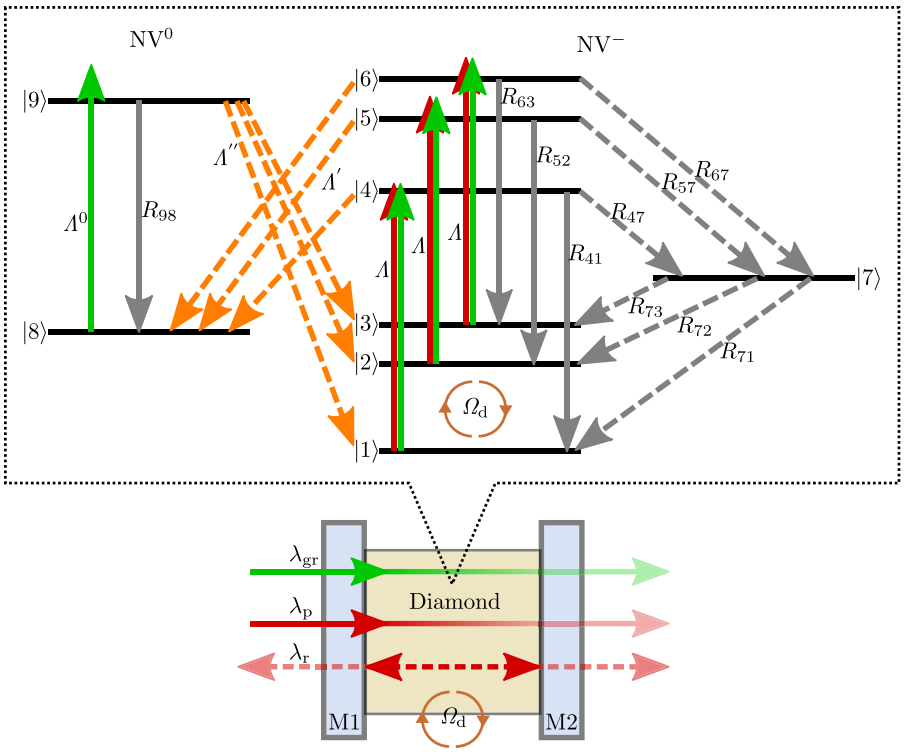

Figure 1. Schematic of the Raman laser with a diamond crystal containing MW driven NV$^-$ centres including the charge state switching between NV$^-$ and NV^0 in the Fabry–Perot cavity. The Fabry–Perot cavity is formed by two highly reflective mirrors denoted as M1 and M2. Directions of the pump (λ_p) and Raman (λ_r) wavelengths are shown in solid and dotted red arrows respectively. The pump is considered as a single pass pump, i.e. the cavity mirrors are not reflective for the pump wavelength. The pump intensity depletes while propagating through the diamond and the light at the Raman wavelength is generated. The Raman wavelength forms a cavity mode and a laser signal is generated. The laser output is transmitted through both mirrors. A level structure model of the MW driven NV$^-$ centre including charge state switching present in the diamond is shown in the inset. Please note that the separation between the levels of both charge states are not in energy difference scale for a clear representation of transitions. Solid red and green upward arrows represent the optical pumping of the NV centres by the λ_p and λ_{gr} wavelengths respectively. The solid and dashed grey downward arrows represent radiative and non radiative (via the singlet state) decay paths. The dashed orange arrows represent light induced charge state switching between NV$^-$ and NV^0. Brown arrows denote the coherent MW driving of the NV$^-$ centre with MW driving frequency Ω_d. The transition rate for each transition are denoted next to the corresponding arrow (please see section 2.2 for more details).

its ground state to excited state with a total pumping rate $\Lambda = \Lambda_p + \Lambda_{gr}$, where the $\Lambda_{p/gr}$ is the corresponding pumping rate of $\lambda_{p/gr}$. This incoherent optical excitation occurs via spin conserving transitions ($\Delta m_s = 0$) and hence excites the NV centre from states $|1\rangle|2\rangle$, and $|3\rangle$ to states $|4\rangle$, $|5\rangle$, and $|6\rangle$ respectively. These incoherent optical transitions in fact involve phonon levels of excited states $|4\rangle$, $|5\rangle$, and $|6\rangle$, but since those phonon levels have extremely short lifetime [59], compared with that of $|4\rangle$, $|5\rangle$, and $|6\rangle$, we neglect them for simplicity. Since this incoherent laser pumping is spin conserving, the linewidth of the laser used is not critical for NV$^-$ centre system. We treat appreciable coherence only between the $|1\rangle$ and $|2\rangle$ and assume an intrinsic dephasing rate, Γ_g between these levels. This intrinsic dephasing rate (Γ_g) of the NV$^-$ centre ground state is assumed to be 1 MHz unless specified otherwise [1, 24]. We also consider the effect of laser pumping rates Λ_p and Λ_{gr} on this transition and neglect the spin relaxation since continuous laser and MW driving determine the spin dynamics on a faster time scale. For the light induced transitions, the transition rate is determined by the intensity of the light, cross-section of the transition and the energy of a photon at the wavelength of the light (transition rate = intensity × cross-section of the transition/energy of a photon). We consider the absorption cross-section for λ_{gr} as $\sigma_{gr} = 3.1 \times 10^{-17}$ cm^{-2} [60]. The absorption cross-section, σ_p of the NV$^-$ centre for the considered pump wavelength (λ_p) is approximately 1.31×10^{-17} cm^2, which we obtain from scaling the σ_{gr} for 532 nm with a measured absorption spectrum to the wavelength in question [22]. This value of absorption cross-section is reasonable since a slightly lower value of 1.1×10^{-17} cm^2 for NV$^-$ centre at 632 nm is reported in [45].

The NV$^-$ centre population from $|4\rangle$, $|5\rangle$, and $|6\rangle$ spontaneously decay to the ground state via two path ways [1, 58]. The first one, involves spin-conserving optical transitions emitting near-IR photons, from $|4\rangle$, $|5\rangle$, and $|6\rangle$ to $|1\rangle$, $|2\rangle$, and $|3\rangle$, respectively. The second one, via non spin-conserving transitions from $|4\rangle$, $|5\rangle$, and $|6\rangle$ to $|1\rangle$, $|2\rangle$, and $|3\rangle$ through $|7\rangle$. The transition rate corresponding to transition $|i\rangle$ to $|j\rangle$ is denoted as R_{ij}. In this study, we consider NV transition rates as $R_{41} = R_{52} = R_{63} = 66.16\ \mu s^{-1}$, $R_{57} = R_{67} = 91.8\ \mu s^{-1}$,

$R_{47} = 11.1\ \mu s^{-1}$, $R_{71} = 4.87\ \mu s^{-1}$, $R_{72} = R_{73} = 2.04\ \mu s^{-1}$ [4, 61]. Here we assume that the transition rates are not affected by the magnetic field [62], though there are indications that they may vary with the external magnetic field [58, 63]. Furthermore, we neglect any stimulated emission of NV centres at λ_r [25, 26, 51], since no direct evidences of stimulated emission below 700 nm is experimentally reported so far to the best of our knowledge. Moreover, experimental study in [25] indicated that for a wavelength above 680 nm, the stimulated emission dominates over the ionization and the cross-over wavelength is close to 660 nm. In the light of this, our model seems reasonable.

We consider the ionization transition from $|4\rangle$, $|5\rangle$ and $|6\rangle$ to $|8\rangle$ and the recombination transitions from $|9\rangle$ to $|1\rangle$, $|2\rangle$ and $|3\rangle$ [26, 49, 51, 64, 65]. We represent the ionization transition rate and cross-sections for $\lambda_{gr/p/r}$ as $\Lambda'_{gr/p/r}$ and $\sigma'_{gr/p/r}$ respectively. Similarly, we represent the recombination transition rate and cross-sections for $\lambda_{gr/p/r}$ as $\Lambda''_{gr/p/r}$ and $\sigma''_{gr/p/r}$ respectively. Since we consider that all three wavelengths in the present study induces the charge state switching, we denote the total ionization and recombination transition rates as $\Lambda' = \Lambda'_{gr} + \Lambda'_{p} + \Lambda'_{r}$ and $\Lambda'' = \Lambda''_{gr} + \Lambda''_{p} + \Lambda''_{r}$ respectively. We assume that each of the transitions from $|4\rangle$, $|5\rangle$ and $|6\rangle$ to $|8\rangle$ has a transition rate of $\Lambda\prime$ and are not spin dependent transitions [28, 64, 65]. Experimental study with nanodiamond NV centre in [66] reported that this ionization transition can be directly spin dependent. Similarly, we assume that each of the transitions to $|1\rangle$, $|2\rangle$ and $|3\rangle$ from $|9\rangle$ has a transition rate of Λ'' [28, 64, 64, 66].

We consider $\sigma'_{gr/p} = \eta'_{gr/p} \times \sigma_{gr/p}$ and $\sigma''_{gr} = \eta''_{gr/p} \times \sigma_{gr/p}$, where $\eta'_{gr} = 0.037$ and $\eta''_{gr} = \frac{1}{3} \times 0.08$ [51]. Please note that the wavelength considered in [51] is 531 nm. The factor $\frac{1}{3}$ in the η''_{gr} considers that there are three transition from $|9\rangle$, which was considered as a single transition in [51]. The ionization and recombination transitions are expected to be wavelength dependent since the probability of removing electrons from NV^- centres or charge donors like P1 centres can be directly proportional to the energy of the photon [52]. Due to the lack of experimental evidences to the best of our knowledge, we assume $\eta'_{p} = \eta'_{gr}$ and $\eta''_{p} = \eta''_{gr}$, and also assume that the frequency dependence σ'_{p} and σ''_{p} comes through the absorption cross-section part. We expect $\sigma'_{p} > \sigma'_{r}$ and $\sigma''_{p} > \sigma''_{r}$ since the λ_p photon is more energetic than that of λ_r. However, for simplicity of the calculation and also for not underestimating the charge state switching between NV^- and NV^0 due to the strong intra-cavity field at λ_r, we assume $\sigma'_{p} = \sigma'_{r}$ and $\sigma''_{p} = \sigma''_{r}$. The charge state switching can be tuned in principle via material engineering of the diamond [55, 56, 67]. The NV^0 is excited by the λ_{gr} and we consider that the pumping rate for this is $\Lambda^0 = 1.3 \times \Lambda_{gr}$ [51]. The spontaneous emission rate of NV^0 is considered as $R_{98} = 53\ \mu s^{-1}$ [28, 51, 64, 68]

Since the absorption of the λ_p by NV^- centre happens from both levels $|1\rangle|2\rangle$, and $|3\rangle$, their populations determine the intra-cavity absorption by NV^- centres per crystal length, which is relevant to the Raman laser model in the following section. To obtain populations, the master equation for the density matrix ρ of the NV^- centre together with NV^0 centre from the nine-level system can be written as [24, 69–71],

$$\frac{d\rho_{12}}{dt} = (i\Delta_g - \Lambda - \Gamma_g)\rho_{12} - i\frac{\Omega_d}{2}(\rho_{22} - \rho_{11}), \tag{1}$$

$$\frac{d\rho_{21}}{dt} = -(i\Delta_g + \Lambda + \Gamma_g)\rho_{21} - i\frac{\Omega_d}{2}(\rho_{11} - \rho_{22}), \tag{2}$$

$$\frac{d\rho_{11}}{dt} = -i\frac{\Omega_d}{2}(\rho_{21} - \rho_{12}) - \Lambda\rho_{11} + R_{41}\rho_{44} + R_{71}\rho_{77} + \Lambda''\rho_{99}, \tag{3}$$

$$\frac{d\rho_{22}}{dt} = i\frac{\Omega_d}{2}(\rho_{21} - \rho_{12}) - \Lambda\rho_{22} + R_{52}\rho_{55} + R_{72}\rho_{77} + \Lambda''\rho_{99}, \tag{4}$$

$$\frac{d\rho_{33}}{dt} = -\Lambda\rho_{33} + R_{63}\rho_{66} + R_{73}\rho_{77} + \Lambda''\rho_{99}, \tag{5}$$

$$\frac{d\rho_{44}}{dt} = \Lambda\rho_{11} - (R_{41} + R_{47})\rho_{44} - \Lambda'\rho_{44}, \tag{6}$$

$$\frac{d\rho_{55}}{dt} = \Lambda\rho_{22} - (R_{52} + R_{57})\rho_{55} - \Lambda'\rho_{55}, \tag{7}$$

$$\frac{d\rho_{66}}{dt} = \Lambda\rho_{33} - (R_{63} + R_{67})\rho_{66} - \Lambda'\rho_{66}, \tag{8}$$

$$\frac{d\rho_{77}}{dt} = R_{47}\rho_{44} + R_{57}\rho_{55} + R_{67}\rho_{66} - (R_{73} + R_{72} + R_{71})\rho_{77}, \tag{9}$$

$$\frac{d\rho_{88}}{dt} = \Lambda'(\rho_{44} + \rho_{55} + \rho_{66}) - \Lambda^0\rho_{88} + R_{98}\rho_{99}, \tag{10}$$

$$\frac{d\rho_{99}}{dt} = \Lambda^0\rho_{88} - 3\Lambda''\rho_{99} - R_{98}\rho_{99}, \tag{11}$$

where $\sum_i \rho_{ii} = 1$.

The steady-state solution yields the total ground-state population, $\rho_g = \rho_{11} + \rho_{22} + \rho_{33}$ of the NV^- centre. Then we can write the exponential absorption per unit length, $\beta = \sigma_p D \rho_g$, where D is the density of NV^- centres in the diamond crystal, respectively. Note that we define β as an exponent of e, while literature values are often given as an exponent of 10.

In order to discuss the underlying physics in a simplified manner, we neglect the populations in the levels $|3\rangle$ and $|6\rangle$, and also the charge state switching for now, but we consider them for the rest of this article. For a particular Λ and Ω_d, the resonant MW driving ($\Delta_g = 0$) evenly distributes the ground-state population of NV^- centres between $|1\rangle$ and $|2\rangle$ at steady state. On the other hand, the non-resonant MW driving ($\Delta_g \neq 0$) unevenly distributes the NV^- ground-state population, preferring $|1\rangle$ over $|2\rangle$. Magnetic sensing based on NV^- absorption [28, 30, 31] is based on the key fact $R_{57} > R_{47}$. Thus at a particular Λ and Ω_d, more NV^- centre population reaches the singlet level $|7\rangle$, for resonant MW driving ($\Delta_g = 0$), in comparison with the non-resonant MW driving ($\Delta_g \neq 0$), where population ends up mainly in state $|1\rangle$ and $|4\rangle$. Since $|7\rangle$ has a relatively longer lifetime than that of excited-state levels, the ground-state population ρ_g at steady-state for resonant MW driving is lower than that of non-resonant MW driving [28, 30, 31]. As a result, the absorption is higher for detuned MW driving ($\Delta_g \neq 0$) than that of resonant MW driving ($\Delta_g = 0$). Since an external magnetic field induces detuning through Zeeman splitting, the absorption is also modified by such an external magnetic field and thus enables magnetic sensing.

2.2. Diamond Raman laser with NV^- centres as absorbers in the crystal

We consider a Raman laser generating light from Raman scattering off a diamond crystal containing also NV^- (and NV^0) centres in a Fabry–Perot cavity with pumping at a wavelength (λ_p) below the ZPL (schematic is shown in figure 1). We follow modelling the Raman laser in an approach similar to [72, 73]. However, the important difference is the consideration of pump absorption, which otherwise is negligible in Raman laser modelling [73].

We simplify the system with the following assumptions: both mirrors, M1 and M2 are identical, and highly reflective only for the first Raman wavelength, but fully transmitting any other wavelengths like the pump (λ_p) as well as all higher-order Raman wavelengths, λ_{gr} etc. NV^- (and NV^0) centres are uniformly distributed through the diamond volume in the cavity and the cavity is fully filled with the diamond sample. We neglect all contributions into the cavity mode from spontaneous Raman emission as well as spontaneous emission from the NV centres, since the stimulated Raman emission dominates above threshold. We approximate the fundamental Gaussian cavity mode by a cylinder shape, where the base radius of the cylinder is the cavity beam waist and also approximate the transverse profile to a flattop profile.

The Raman gain for the stimulated Raman scattering is $g_r I_p I_r$ [72–75], where g_r is the plain Raman gain coefficient, I_p is the intensity of the pump beam, and I_r is the intensity of the Raman beam. Then the depletion of the pump when it propagates through the diamond position l can be written as [73],

$$\frac{dI_p}{dl} = -\frac{\nu_p}{\nu_r} g_r I_p(l) I_r - \beta I_p(l), \tag{12}$$

where ν_p and ν_r are pump and Raman frequencies corresponding to (λ_p) and (λ_r) respectively. Here, $\beta = \sigma_p D \rho_g$ represents the pump absorption, I_r is approximated to be uniform throughout the cavity and $I_p(l)$ is a function of length l. Strictly speaking the pump absorption $\beta = \sigma_p D \rho_g$ is also a function of position l, since different pump intensities $I_p(l)$ lead to different levels of saturation and thus ground state population $\rho_g(l)$. Mathematically this dependence manifests itself in the master equation through the pump rate $\Lambda_p(l) = \sigma I_p(l)/h\nu_p$. This dependence of β on length makes equation (12), difficult to solve together with a coupled set of master equations from (1) to (11). However, based on a relatively weak reduction of the pump in a single pass and in order to separate the temporal and spatial variables in the differential equations, we assume that β is a constant over the length of the cavity. For this, we make the approximation that $\Lambda_p(l) = \Lambda_p \sim \sigma I_p^0/h\nu_p$, where I_p^0 is the intensity of the pump entering to the cavity through M1. Since I_p^0 is the maximum intensity of the pump wavelength in the cavity, the pump rate that we consider is the maximum value. The resultant absorption is higher than the actual scenario and as a result the phase noise to the NV^- centres' ground state coherence considered is also high. However, this approximation enables us to make a good estimate of the Raman laser output generation. The solution of equation (12) gives $I_p(l)$ as,

$$I_p(l) = I_p^0 \exp -l\left(\frac{\nu_p}{\nu_r} g_r I_r + \beta\right). \tag{13}$$

If l_c is the cavity length, then the depleted intensity of the pump when it passes through the diamond sample can be written as,

$$\Delta I_p = I_p^0 \left[1 - \exp -l_c \left(\frac{\nu_p}{\nu_r} g_r I_r + \beta\right)\right]. \tag{14}$$

Following the method in [73], the total intensity of stimulated Raman emission generated in a single pass from equation (14) can be written as,

$$\Delta I_r = \frac{g_r I_r}{\frac{\nu_p}{\nu_r} g_r I_r + \beta} \Delta I_p. \tag{15}$$

The temporal rate of Raman generation is $(c/n)\Delta I_r/l_c$ [72], where c and n are the speed of light and the refractive index of the diamond respectively. Hence, the temporal rate equation for the Raman laser intensity inside the cavity can be written as,

$$\frac{dI_r}{dt} = \frac{c/n}{l_c} \Delta I_r - \kappa_r I_r, \tag{16}$$

where t represents time and κ_r is the cavity loss rate through the mirror transmissions. Using equations (14)–(16), the I_p^0 at steady state can be written as,

$$I_p^0 = \frac{\frac{l_c}{c/n}\kappa_r}{\frac{g_r}{\frac{\nu_p}{\nu_r} g_r I_r + \beta}\left[1 - \exp -l_c \left(\frac{\nu_p}{\nu_r} g_r I_r + \beta\right)\right]}. \tag{17}$$

Equation (17) gives a relation between the incident pump intensity I_p^0 and the intra-cavity Raman laser intensity I_r. The intensity of the Raman laser output (I^{out}) emitted from the cavity can, then be written as,

$$I_r^{out} = \frac{l_c}{c/n} \kappa_r I_r. \tag{18}$$

The pump and the Raman laser output power can be obtained by multiplying respective intensities with the area of the cavity beam (A_{beam}). Then using equations (17) and (18), we have the pump and laser output relation incorporating NV^- absorption. We obtain an analytical solution for β using the steady-state solution of the master equations for ρ_g from section 2.1. This analytical solution is a lengthy one and we do not explicitly write it down here. Since ρ_g is a function of Λ_p, β is a function of I_p^0. Plugging this analytical form for β into equation (17), we numerically solve the combination of equations (17) and (18), to obtain the pump power for each Raman laser output power. Then we numerically study the response of such a laser to external magnetic fields.

3. Results and discussion

We consider a micro-cavity Raman laser that leads to strong intra-cavity light intensity and Raman scattering thereby reducing the laser threshold. An interesting candidate for this would be fibre cavities [26, 76]. We consider the length of the diamond sample l_c as 700 μm and the beam waist radius as 10 μm. We assume a finesse of 10 000, for the diamond loaded cavity, which makes the cavity loss rate $\kappa_r = 56.1$ MHz. For a cavity loaded with a pure diamond sample of around 10 μm thickness, a cavity finesse of around 17 000 has been demonstrated before [77].

Since we are considering a microcavity, for strong pump absorption, we consider a high density of preferentially oriented NV^- centres, $D \sim 7 \times 10^{17}$ cm^{-3}, that has been experimentally realized [78]. Diamonds with even higher density of NV^- centres, but not preferentially oriented have been shown in experiment [45, 79, 80]. The Raman gain (g_r) for the choice of our wavelength is around 14.75 cm GW^{-1} [33, 81].

3.1. Raman laser LTM

An example of numerical solutions of the Raman laser output as a function of pump laser power, for different MW driving conditions, is shown in figure 2. Since the absorption by NV^- centres is less for the resonant MW driving ($\Delta_g = 0$) than for detuned MW driving ($\Delta_g \neq 0$) or MW-off case ($\Omega_d = 0$), the resonant case reaches the threshold for lower pump powers than the detuned case or MW-off case. As the detuning Δ_g increases, the laser curves tends towards that of the MW-off case. The threshold corresponding to the MW-off case is fundamentally limited by the number of NV^- centres in the cavity volume and their internal transition rates. In figure 2, the laser curve corresponding to resonant MW driving is linear, but as the detuning increases, laser curves become non-linear and for the MW-off case we can see a bistable behaviour [46–48] in the Raman laser output. We identify that this transition from linear to non-linear laser curves as we move from resonant MW

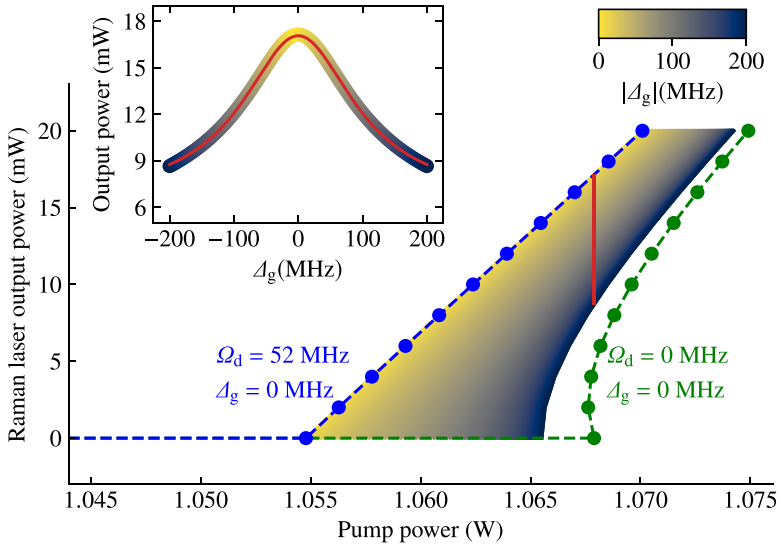

Figure 2. Raman laser output power in milli-Watt (mW) as a function of pump power, for $\Lambda_{gr} = 21$ MHz and for different MW driving conditions. The blue dots are the numerically obtained solutions of Raman-laser output power for resonant MW driving ($\Delta_g = 0$ MHz) with $\Omega_d = 52$ MHz. The green dots are the solutions when no MW field driving is present ($\Omega_d = 0$ MHz). The dashed curves are interpretation laser curves considering that the Raman laser output power should be zero when the pump power is zero. The gradient shaded region is formed by joining the line plots of numerical solutions corresponding to different Δ_g from 0 to 200 MHz for $\Omega_d = 52$ MHz. For a pump power equal to the threshold pump power of the MW-off laser curve, the Raman-laser output changes through the red line cut. Raman-laser output as a function of detuning is shown in the inset. The data points are shown in the corresponding gradient colour in the main figure. The red curve in the inset is a Lorentzian function fit.

driving to non-resonant MW driving(or MW-off case) arises basically due to the transition from linear increase to non-linear decrease in the steady state ground state population ρ_g (and thereby β) when the strong intra-cavity field at λ_r increases. Since we are working with the Raman laser that is already turned on, the bistability behaviour is not expected to affect the present magnetometry scheme. Furthermore, due to the high finesse of 10 000 for the cavity, the intra-cavity power corresponding to 18 mW Raman laser output power (multiplying with finesse/π) can be roughly estimated to be around 57 W and thus one has to be careful about the damage threshold for experimental studies.

We can apply the LTM method to detect the external magnetic field by assuming that the MW frequency for driving the NV^- centre is constant at a fixed value and the detuning is induced by some external magnetic field [24]. For this, we set the pump power to P'_p, which is the upper threshold value (green curve) in the main figure 2 [28]. Then looking at the change in the Raman laser output for resonant MW driving corresponding to P'_p pump power, we can infer the detuning and thereby the magnetic field present, since $B_{DC} = \Delta_g/\gamma_e$, where $1/\gamma_e = 5.68 \times 10^{-12}$ T Hz^{-1} [24]. For the rest of the study we consider Δ_g between 0 MHz and 200 MHz for numerical estimations. The output power of the Raman laser as a function of the detuning then forms a peak around zero, as shown in the inset figure of figure 2, since at resonance the absorption is the lowest. The numerical solution of output power of the Raman laser as a function of the detuning can be fitted with a Lorentzian line-shape function of the form (amplitude $\times$ 0.25 $\times$ $FWHM^2/(\Delta_g^2 + 0.25 \times FWHM^2)) + C$, where FWHM and C are the full-width at half maximum and a constant respectively. For $\Delta_g < 0$, the curve in the inset mirrors with respect to $\Delta_g = 0$. Since we require only $|B_{DC}|$ for estimating the DC magnetic field, we focus on the positive values of Δ_g. The peak width of this curve is set by the power broadening and phase noise that arises due to the Rabi driving Ω_d, dephasing rate Γ_g, and laser pumping Λ, to the NV^- ground state coherence. In addition the charge state switching is also expected to contribute to this peak width. The laser pumping Λ is determined by the Λ_{gr}, since we have assumed fixed cavity parameters that roughly fixes the pump powers and thereby the contribution from Λ_p. We explore the effects of MW driving, Ω_d, Λ_{gr} and Γ_g in figure 3.

Since we are fixing the pump power to P'_p and looking at the Raman laser output change, any undesired fluctuations in the pump power is expected to produce noise in the Raman laser output power masking the magnetic-field signal we want to detect. Thus in experiments, it is important to work with a pump laser that is stabilized for power. As a result it is interesting to maximise the threshold shift between resonant ($\Delta_g =$ 0 MHz) and off-resonant driving ($\Delta_g = 200$ MHz). We therefore explore the threshold pump power shift of the Raman laser as a function of Rabi driving Ω_d and laser pumping Λ_{gr} in figure 3(a). We choose a region of values for the Ω_d and Λ_{gr} such that there is significant recombination transition from NV^0 to NV^- and in result includes a percentage shift more than 1% as shown in figure 3(a). Both laser pumping Λ_{gr} and Ω_d show

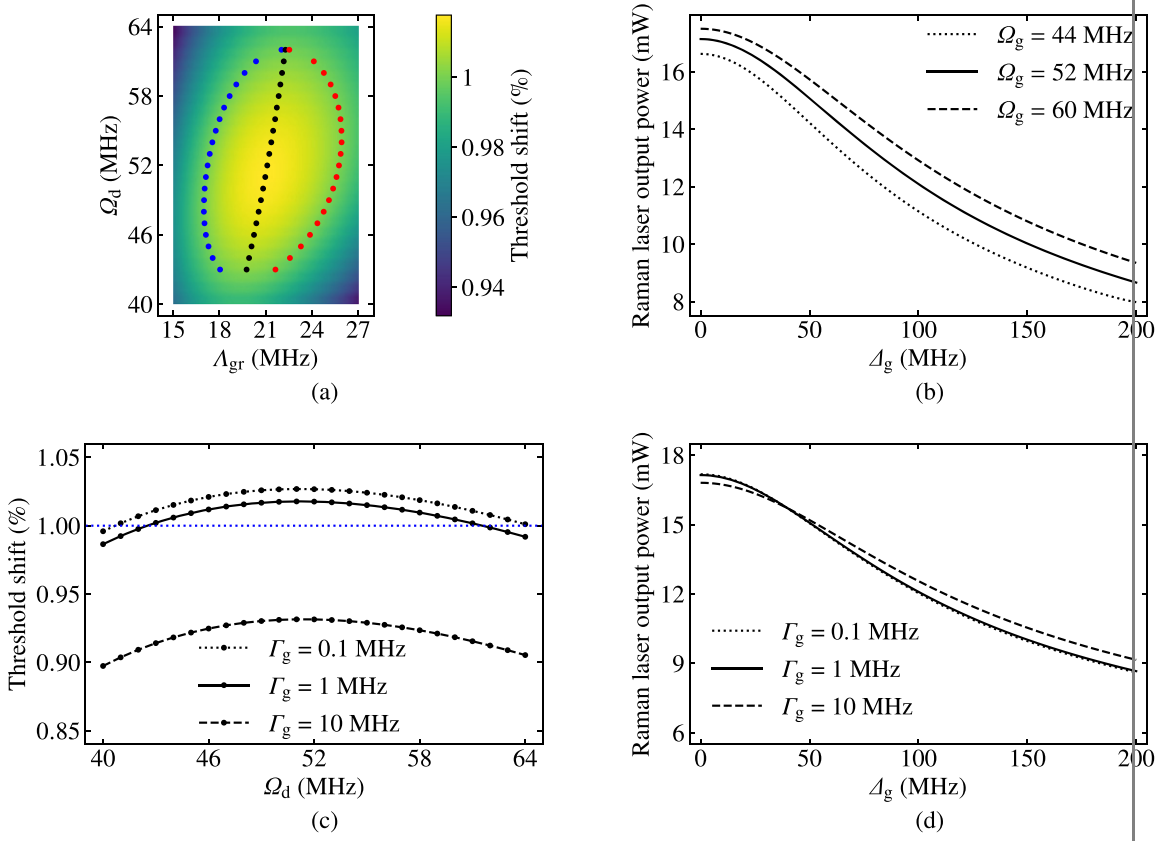

Figure 3. (a) The shift in threshold pump power for detuned laser curves ($\Delta_g = 200$ MHz) with respect to that of resonant laser curves ($\Delta_g = 0$ MHz) as a percentage of threshold pump power of resonant laser curves as a function of Ω_d and Λ_{gr}. The threshold pump power for resonant driving is roughly between 1.065 W (for $\Omega_d = 40$ MHz and $\Lambda_{gr} = 15$ MHz) and 1.046 W (for $\Omega_d = 64$ MHz and $\Lambda_{gr} = 27$ MHz). The blue and red dots highlight the minimum and maximum values for Λ_{gr} that has $\geqslant$1% threshold shift corresponding to each Ω_d values. The black dots highlight the Λ_{gr} and Ω_d values that corresponds to optimum threshold shift. Γ_g is 1 MHz. (b) Raman-laser output power as a function of Δ_g for $\Lambda_{gr} = 21$ MHz, $\Gamma_g = 1$ MHz, and for different values of Ω_d (numerical solutions as line plots). (c) Threshold shift as in (a), now as a function of Ω_d for $\Lambda_{gr} = 21$ MHz, and for different values of Γ_g. The dots are the numerical solutions and the dotted, solid, and dashed lines are joining respective numerical solutions. (d) Raman laser output as a function of Δ_g for $\Lambda_{gr} = 21$ MHz, $\Omega_d = 52$ MHz, and for different values of Γ_g (numerical solutions as line plots).

characteristic maximum (i.e. optimum). One hand, increasing Λ_{gr}, the recombination transition is expected to increase, which brings more NV^- ground state population. On the other hand, increasing Λ_{gr} the excitation of the NV^- and ionization transition is expected to increase. As a result an optimum value for the laser pumping Λ_{gr} is expected. The P'_p roughly varies from 1.076 W ($\Lambda_p \sim 13.89$ MHz) to 1.06 W ($\Lambda_p \sim 13.68$ MHz) as Λ_{gr} varies from 15 MHz to 27 MHz, since the threshold pump power corresponds to the MW-off case changes with Λ_{gr}.

In order to understand the optimised effect of MW driving Ω_d in the threshold shift, we consider the laser pumping $\Lambda_{gr} = 21$ MHz and plot the Raman laser output curve as a function of Δ_g for different values of Ω_d as shown in figure 3(b). Figure 3(b), shows that increasing Ω_d improves the Raman laser output, but broadens the resonance peak. The resonance peak broadening for higher Ω_d is expected due to the significant contribution into phase noise to the ground state coherence by Ω_d [82]. The effect of Γ_g explored in figures 3(c) and (d) shows that improving Γ_g by an order of magnitude from 1 MHz does not really improve anything. On the other hand, increasing Γ_g by an order of magnitude changes both threshold shift and the Raman laser output resonance peak width. We attribute this effect to the fact that Λ is the dominant source of phase noise to the ground state coherence and increasing the Γ_g by an order of magnitude from 1 MHz makes Γ_g comparable to Λ.

3.2. Sensitivity of the present magnetometry scheme and its optimisation

The dominant and limiting noise in the magnetic field sensing using the present scheme is expected to be the photon-shot noise and thus we estimate a photon-shot noise limited magnetic field sensitivity of the system [2, 3, 24]. If the Raman laser output (P_r^{out}) varies by an infinitesimally amount dP_r^{out} corresponding to an infinitesimally small change dB_{DC} in the DC magnetic field, for a finite measurement time dt, then the photon-shot noise and the signal photon number that informs about the magnetic field can be written as $\sqrt{(P_r^{out}/h\nu_r)dt}$

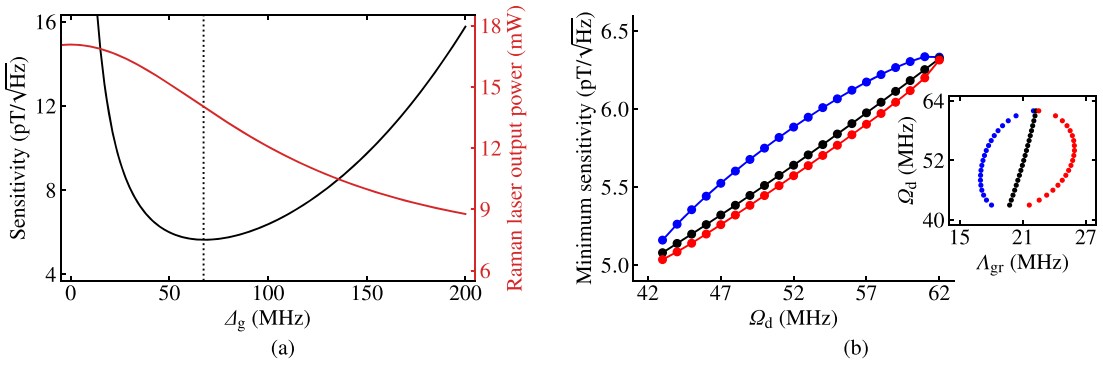

Figure 4. Sensitivity estimation of the present scheme. (a) The sensitivity (black curve) varies as a function of the MW detuning Δ_g, and reaches a minimum value (best sensitivity) at the dotted vertical line. The sensitivity is calculated from the Raman laser output (red curve and axis), obtained by the Lorentzian fit function to the data as shown in figure 2. The sensitivity increases towards zero detuning as the slope in the red curve tends to zero. (b) The numerical solutions of the minimum sensitivity for the Ω_d and Λ_{gr} values from figure 3(a) (reproduced here in the inset). These were obtained for $\Gamma_g = 1$ MHz. The sensitivity is lower (better) for smaller Ω_d (left side of plot) and for larger Λ_{gr} values (red curve).

and $(\mathrm{d}P_r^{out}/h\nu_r)\mathrm{d}t$ respectively. Then the photon-shot noise limited sensitivity ($\eta_{DC} = |\mathrm{d}B_{DC}|\sqrt{\mathrm{d}t}$) to the DC magnetic field B_{DC} can be written from equating the signal photon number to the photon shot noise as [2, 3], $\eta_{DC} = \sqrt{h\nu_r P_r^{out}} \times |\mathrm{d}B_{DC}/\mathrm{d}P_r^{out}|$. The derivative $|\mathrm{d}B_{DC}/\mathrm{d}P_r^{out}|$ can be obtained as the inverse of the slope of the laser output curve as a function of detuning using the gyromagnetic ratio (γ_e) of the NV$^-$ centre. We estimate and explore the minimum sensitivity of the present magnetometry scheme as shown in figure 4.

The sensitivity corresponding to the Raman laser presented in figure 2 as a function of detuning is shown in figure 4(a). To better determine the slope of the Raman laser output curve as a function of detuning, we use Lorentzian fit function of the numerical solutions (red colour curve in figure 2 inset). The derivative of the obtained interpolation function is used to estimate the sensitivity. Close to zero detuning the laser is not sensitive to the external magnetic field since the slope of the laser output goes to zero. The optimal magnetic field sensitivity is at a specific detuning value simply found by minimising the expression $\eta_{DC} = \sqrt{h\nu_r P_r^{out}} \times |\mathrm{d}B_{DC}/\mathrm{d}P_r^{out}|$, i.e. maximising the slope of the red curve in figure 4(a) divided by the square root of the power output $(|\mathrm{d}P_r^{out}/\mathrm{d}\Delta_g|)/\sqrt{P_r^{out}}$. The minimum sensitivity obtained in figure 4(a) is around 5.64 pT $\sqrt{\mathrm{Hz}^{-1}}$ for a Δ_g of around 67 MHz. Furthermore, the sensitivity can be slightly improved close to 4 pT $/\sqrt{\mathrm{Hz}}$ if we reduce the pump power of λ_p, towards the threshold of the 200 MHz detuned laser curve.

To explore the effect of Ω_d and laser pumping Λ_{gr} on the minimum sensitivity, we consider Rabi driving Ω_d and laser pumping Λ_{gr} values which give a threshold shift $\geqslant$1%. These are the points shown in blue, black and red colours in figure 3(a), and are reproduced inset to figure 4(b) for clarity. The corresponding optimum sensitivities are shown in figure 4(b) as a function of Ω_d. The minimum sensitivity increases for the Ω_d in the considered domain, and we attribute this to the noise on the ground state coherence due to MW power broadening as we discussed above. On the contrary, increasing the laser pumping Λ_{gr} decreases (improves) the minimum sensitivity as shown by moving from the blue to red curves. However, this effect is not linear and we attribute this to competing mechanisms. On one hand, increasing Λ_{gr} should increase the noise on the ground state coherence and increase the ionization transition due to the excitation of NV$^-$. On the other hand, increasing Λ_{gr} will enhance the recombination transitions and also allow a reduction of Λ_p due to the reduced threshold pump power, which can reduce noise to the system. The results shown in figure 4(b) suggest that the second situation dominates. To see the effect of lower Ω_d values on the minimum sensitivity, we keep the $\Lambda_{gr} =$ 21 MHz and explored the minimum sensitivity as a function of Ω_d. The sensitivity slightly improves as the Ω_d reduces further from the region shown in figure 4(b) and reaches an optimum value of about 4.16 pT $/\sqrt{\mathrm{Hz}}$ for $\Omega_d = 20$ MHz. However, the threshold shift (as in figures 3(a) and (c)) for this is only about 0.67% and thus we expect significant technical noise due to the challenge in stabilizing the pump power. Reducing Ω_d further makes the minimum sensitivity worse as an effect of weak coherent MW driving of the ground state population (reduces the contrast of the resonance peak of the Raman laser output as a function of detuning).

To estimate the sensitivity advantage of a diamond Raman LTM cavity we benchmark our scheme with conventional ODMR NV$^-$ magnetometry. In conventional ODMR, the volume defined sensitivity ($\eta_{DC} \times \sqrt{\text{sensing volume}}$), with a diamond sample having 2 ppm NV$^-$ density and a comparable dephasing rate is about 100–200 nT $\sqrt{\mu\mathrm{m}^3\ \mathrm{Hz}^{-1}}$ (see figure 10.F [83]). The number of NV$^-$ centres in this conventional magnetometry sensing volume would be equal to the number of NV$^-$ + NV^0 centres that we considered in our cavity, if its sensing volume is around 2 times larger than our cavity volume (around $2.2 \times 10^{-4}\ \mu\mathrm{m}^3$). Then the sensitivity, η_{DC} of the conventional magnetometry is roughly around $150 - 300$ pT $/\sqrt{\mathrm{Hz}}$, which is roughly

two orders of magnitude worse than the sensitivities we estimated in the present work. Thus we can conclude that comparing the two techniques with both CW laser and CW MWs, the absorptive diamond Raman laser cavity in our scheme results in a sensitivity advantage of two orders of magnitude.

The sensitivity of conventional NV^- magnetometry can further be improved by switching from CW techniques to pulsed and/or lock-in techniques. Focussing only on the sensitivity value, an experimental DC sensitivity with NV^- centres of about 15 pT $/\sqrt{\text{Hz}}$ [84] was demonstrated in 2016. Very recently using a magnetic flux concentrator this was improved to about 0.9 pT $/\sqrt{\text{Hz}}$ [85] and using improved pulsed sequences [86] this has been further reduced to about 0.5 pT $/\sqrt{\text{Hz}}$. In principle these advantages such as a flux concentrator could be combined with LTM schemes. However, in order to combine pulsed schemes with a laser read-out of NV^- centres, questions of cavity build-up times and their interference with the read-out times arise. Dynamical calculations are therefore needed to discuss sensitivities of such combinations and the steady-state solutions presented in this paper are not sufficient.

Comparing our scheme to other LTM schemes, naively we can say that the minimum sensitivity we obtain, is slightly worse than the 0.7 pT $/\sqrt{\text{Hz}}$, projected DC sensitivity for IR LTM in [28], and is a few orders of magnitude worse than the projected one for the NV^- LTM [24]. The dephasing rates considered in these works fall within the values we consider in this work. However, a proper comparison should consider the total number of NV^- centres involved, i.e. the diamond volume and the density of NV^- centres in different schemes. For application advantages, such as low-power operation and fibre-coupling we chose a microcavity with a diamond sensing volume of $\pi \times (10\,\mu\text{m})^2 \times 700\,\mu\text{m} = 2.2 \times 10^{-4}\,\mu\text{m}^3$. The IR LTM scheme assumed a diamond volume that is larger by a factor around 3.6 ($\pi \times (50\,\mu\text{m})^2 \times 100\,\mu\text{m}$) and the $NV^- + NV^0$ density larger by a factor of 4 [28] than the present case. The active NV^- lasing scheme assumed 1 mm^3 of diamond sensing volume with an NV density larger by a factor 4 than the present case.

In LTM schemes, the optical cavity parameters can influence the laser output and threshold shift and thus sensitivity. These are additional parameters compared to conventional NV^- magnetometry, where the linewidth is typically defined by the NV diamond material and the only corresponding setup parameter is the photon collection efficiency. These additional parameters can on the one hand be used to adapt a sensor to serve particular requirements such as wide dynamic range versus sensitivity. On the other hand they can make performance fabrication-dependent and thus require more calibration. However, we point out here, that the cavity and fabrication has no influence on the fundamental NV^- centre's magnetic resonance frequency or its shift with the external magnetic field, purely defined by the fundamental gyromagnetic ratio. Thus the main fundamental advantage of NV^- centres over other magnetometer technologies, often labelled 'calibration-free' measurements, is preserved.

4. Conclusion

We have shown that a low threshold single pass pump diamond Raman laser with absorption of only the pump wavelength by MW driven NV^- centres in the same diamond crystal can be used to detect external magnetic fields. The choice of a micro-cavity with high finesse for the Raman wavelength reduces the threshold powers well below NV^- saturation powers and thus could investigate the role of NV^- centres. We have explored the response of such a Raman laser as a function of incoherent laser pumping, MW driving strength, and intrinsic dephasing rate. We find that the laser threshold shifts between on- and off-resonant MW driving of the NV^- centres, which allows for sensing. The threshold shift can be maximized by tuning the green laser pumping Λ_{gr} and MW driving Ω_d, two parameters that can be tuned during experimental study. Furthermore, we have estimated the DC magnetic field sensitivity and explored the effect of different green laser pumping Λ_{gr} and MW driving Ω_d values on the minimum sensitivity. We obtain a minimum sensitivity of down to a few pT $/\sqrt{\text{Hz}}$ and find that for comparable sensing volume, NV^- density and coherence time our scheme gives an advantage of a couple of orders of magnitude in sensitivity compared with conventional ODMR. The sensitivity range projected in this study is comparable with the projected DC magnetic sensitivity of other LTM magnetometry with NV^- centres reported [24, 28], but the conceptual simplicity of our scheme can attract potential applications, especially since it takes advantage of the well-established, visible wavelength Raman lasing properties also provided by diamond.

Acknowledgements

Sarath Raman Nair acknowledges that this work was done while holding the International Macquarie University Research Excellence Scholarship (iMQRES) (Allocation No. 2014108) and also acknowledges the EQUS

Centre Collaboration Award. Lachlan J Rogers is the recipient of an Australian Research Council Discovery Early Career Award (Project No. DE170101371). This research was supported by the Australian Research Council Centre of Excellence for Engineered Quantum Systems (EQUS, CE170100009). Jan Jeske acknowledges funding from the German federal ministry for education and research Bundesministerium für Bildung und Forschung (BMBF) under Grant No. 13XP5063. Andrew D Greentree acknowledges the support of an ARC Future Fellowship (Grant No. FT160100357).

Data availability statement

The data that support the findings of this study are available upon reasonable request from the authors.

ORCID iDs

Sarath Raman Nair https://orcid.org/0000-0002-9081-5750
Lachlan J Rogers https://orcid.org/0000-0003-3545-2595
David J Spence https://orcid.org/0000-0001-5974-853X
Richard P Mildren https://orcid.org/0000-0002-1521-2423
Andrew D Greentree https://orcid.org/0000-0002-3505-9163
Thomas Volz https://orcid.org/0000-0001-9850-4992
Jan Jeske https://orcid.org/0000-0003-3532-506X

References

[1] Doherty M W, Manson N B, Delaney P, Jelezko F, Wrachtrup J and Hollenberg L C L 2013 *Phys. Rep.* **528** 1–45
[2] Rondin L, Tetienne J-P, Hingant T, Roch J-F, Maletinsky P and Jacques V 2014 *Rep. Prog. Phys.* **77** 056503
[3] Degen C L, Reinhard F and Cappellaro P 2017 *Rev. Mod. Phys.* **89** 035002
[4] Barry J F, Schloss J M, Bauch E, Turner M J, Hart C A, Pham L M and Walsworth R L 2020 *Rev. Mod. Phys.* **92** 015004
[5] Dolde F *et al* 2011 *Nat. Phys.* **7** 459–63
[6] Dolde F *et al* 2014 *Phys. Rev. Lett.* **112** 097603
[7] Doherty M W *et al* 2014 *Phys. Rev. Lett.* **112** 047601
[8] Neumann P *et al* 2013 *Nano Lett.* **13** 2738–42
[9] Wrachtrup J and Jelezko F 2006 *J. Phys.: Condens. Matter* **18** S807
[10] McGuinness L P *et al* 2011 *Nat. Nanotechnol.* **6** 358–63
[11] Reineck P, Capelli M, Lau D W M, Jeske J, Field M R, Ohshima T, Greentree A D and Gibson B C 2017 *Nanoscale* **9** 497–502
[12] Miller B S *et al* 2020 *Nature* **587** 588
[13] Maletinsky P, Hong S, Grinolds M S, Hausmann B, Lukin M D, Walsworth R L, Loncar M and Yacoby A 2012 *Nat. Nanotechnol.* **7** 320
[14] Degen C L 2008 *Appl. Phys. Lett.* **92** 243111
[15] Mizuno K, Nakajima M, Ishiwata H, Masuyama Y, Iwasaki T and Hatano M 2018 *AIP Adv.* **8** 125316
[16] McCloskey D J, Dontschuk N, Broadway D A, Nadarajah A, Stacey A, Tetienne J-P, Hollenberg L C L, Prawer S and Simpson D A 2020 *ACS Appl. Mater. Interfaces* **12** 13421
[17] Cole J H and Hollenberg L C L 2009 *Nanotechnology* **20** 495401
[18] Hall L T, Cole J H, Hill C D and Hollenberg L C L 2009 *Phys. Rev. Lett.* **103** 220802
[19] Jeske J, Cole J H, Müller C, Marthaler M and Schön G 2012 *New J. Phys.* **14** 023013
[20] Mamin H J, Kim M, Sherwood M H, Rettner C T, Ohno K, Awschalom D D and Rugar D 2013 *Science* **339** 557–60
[21] Juan M L, Bradac C, Besga B, Johnsson M, Brennen G, Molina-Terriza G and Volz T 2017 *Nat. Phys.* **13** 241–5
[22] Kern M, Jeske J, Lau D W M, Greentree A D, Jelezko F and Twamley J 2017 *Phys. Rev.* B **95** 235306
[23] Ledbetter M P, Jensen K, Fischer R, Jarmola A and Budker D 2012 *Phys. Rev.* A **86** 052116
[24] Jeske J, Cole J H and Greentree A D 2016 *New J. Phys.* **18** 013015
[25] Jeske J *et al* 2017 *Nat. Commun.* **8** 14000
[26] Raman Nair S *et al* 2020 *Nanophotonics* **9** 4505–18
[27] Fraczek E *et al* 2017 *Opt. Mater. Express* **7** 2571–85
[28] Dumeige Y *et al* 2019 *Opt. Express* **27** 1706–17
[29] Wolf T, Neumann P, Nakamura K, Sumiya H, Ohshima T, Isoya J and Wrachtrup J 2015 *Phys. Rev.* X **5** 041001
[30] Walsworth R 2017 Absorbtion-based detection of spin impurities in solid-state spin systems *US Patent* 9658301
[31] Ahmadi S, El-Ella H A, Wojciechowski A M, Gehring T, Hansen J O, Huck A and Andersen U L 2018 *Phys. Rev.* B **97** 024105
[32] Loudon R 2001 *Adv. Phys.* **50** 813–64
[33] Mildren R and Rabeau J 2013 *Optical Engineering of Diamond* (New York: Wiley)
[34] Mildren R P, McKay A, Williams R J and Kitzler O 2014 *Opt. Photonics News* **25** 42–9
[35] Williams R J *et al* 2018 *IEEE J. Sel. Top. Quant. Electron.* **24** 1–14
[36] Mildren R P, Sabella A, Kitzler O, Spence D J and McKay A M 2013 *Opt. Eng. Diam.* 239–76
[37] Kitzler O, McKay A and Mildren R P 2012 *Opt. Lett.* **37** 2790–2
[38] Sabella A, Piper J A and Mildren R P 2010 *Opt. Lett.* **35** 3874–6
[39] Spence D J, Granados E and Mildren R P 2010 *Opt. Lett.* **35** 556–8
[40] Nikkinen J, Savitski V, Reilly S, Dziechciarczyk L, Härkönen A, Kemp A and Guina M 2018 *IEEE Photon. Technol. Lett.* **30** 981–4
[41] Murtagh M, Lin J, Mildren R P, McConnell G and Spence D J 2015 *Opt. Express* **23** 15504–13

[42] Reilly S, Savitski V G, Liu H, Gu E, Dawson M D and Kemp A J 2015 *Opt. Lett.* **40** 930–3
[43] Latawiec P, Venkataraman V, Burek M J, Hausmann B J M, Bulu I and Lončar M 2015 *Optica* **2** 924–8
[44] Beha K, Batalov A, Manson N B, Bratschitsch R and Leitenstorfer A 2012 *Phys. Rev. Lett.* **109** 097404
[45] Subedi S D, Fedorov V V, Peppers J, Martyshkin D V, Mirov S B, Shao L and Loncar M 2019 *Opt. Mater. Express* **9** 2076–87
[46] Zhang D, Yu R, Li J, Ding C and Yang X 2013 *Phys. Lett.* A **377** 2621–7
[47] Zhang L, Zhan L, Qin M, Zou Z, Wang Z and Liu J 2015 *J. Opt. Soc. Am.* B **32** 1113–9
[48] Seidel H 1971 Bistable optical circuit using saturable absorber within a resonant cavity *US Patent* 3610731
[49] Aslam N, Waldherr G, Neumann P, Jelezko F and Wrachtrup J 2013 *New J. Phys.* **15** 013064
[50] Manson N B, Hedges M, Barson M S J, Ahlefeldt R, Doherty M W, Abe H, Ohshima T and Sellars M J 2018 *New J. Phys.* **20** 113037
[51] Hacquebard L and Childress L 2018 *Phys. Rev.* A **97** 063408
[52] Siyushev P, Pinto H, Vörös M, Gali A, Jelezko F and Wrachtrup J 2013 *Phys. Rev. Lett.* **110** 167402
[53] Farrer R G 1969 *Solid State Commun.* **7** 685–8
[54] Goss J P, Briddon P R, Jones R and Sque S 2004 *Diam. Relat. Mater.* **13** 684–90
[55] Doi Y *et al* 2016 *Phys. Rev.* B **93** 081203
[56] Groot-Berning K *et al* 2014 *Phys. Status Solidi a* **211** 2268–73
[57] Edmonds A M, D'Haenens-Johansson U F S, Cruddace R J, Newton M E, Fu K M C, Santori C, Beausoleil R G, Twitchen D J and Markham M L 2012 *Phys. Rev.* B **86** 035201
[58] Tetienne J-P, Rondin L, Spinicelli P, Chipaux M, Debuisschert T, Roch J-F and Jacques V 2012 *New J. Phys.* **14** 103033
[59] Ulbricht R, Dong S, Gali A, Meng S and Loh Z H 2018 *Phys. Rev.* B **97** 220302
[60] Wee T-L, Tzeng Y-K, Han C-C, Chang H-C, Fann W, Hsu J-H, Chen K-M and Yu Y-C 2007 *J. Phys. Chem.* A **111** 9379–86
[61] Gupta A, Hacquebard L and Childress L 2016 *J. Opt. Soc. Am.* B **33** B28–34
[62] Jin L, Pfender M, Aslam N, Neumann P, Yang S, Wrachtrup J and Liu R B 2015 *Nat. Commun.* **6** 8251
[63] Capelli M, Reineck P, Lau D W M, Orth A, Jeske J, Doherty M W, Ohshima T, Greentree A D and Gibson B C 2017 *Nanoscale* **9** 9299–304
[64] Meirzada I, Hovav Y, Wolf S and Bar-Gill N 2018 *Phys. Rev.* B **98** 245411
[65] Meirzada I, Wolf S, Naiman A, Levy U and Bar-Gill N 2019 *Phys. Rev.* B **100** 125436
[66] Roberts R P, Juan M L and Molina-Terriza G 2019 *Phys. Rev.* B **99** 174307
[67] Alkahtani M and Hemmer P 2020 *Opt. Mater. Express* **10** 1224–31
[68] Liaugaudas G, Davies G, Suhling K, Khan R U A and Evans D J F 2012 *J. Phys.: Condens. Matter* **24** 435503
[69] Breuer H P, Petruccione F *et al* 2002 *The Theory of Open Quantum Systems* (Oxford: Oxford University Press)
[70] Jeske J and Cole J H 2013 *Phys. Rev.* A **87** 052138
[71] Vogt N, Jeske J and Cole J H 2013 *Phys. Rev.* B **88** 174514
[72] Ding S *et al* 2006 *Appl. Phys.* B **85** 89–95
[73] Kitzler O, McKay A, Spence D J and Mildren R P 2015 *Opt. Express* **23** 8590–602
[74] Penzkofer A, Laubereau A and Kaiser W 1979 *Prog. Quantum Electron.* **6** 55–140
[75] Pask H M 2003 *Prog. Quantum Electron.* **27** 3–56
[76] Hunger D, Steinmetz T, Colombe Y, Deutsch C, Hänsch T W and Reichel J 2010 *New J. Phys.* **12** 065038
[77] Janitz E, Ruf M, Dimock M, Bourassa A, Sankey J and Childress L 2015 *Phys. Rev.* A **92** 043844
[78] Ozawa H, Hatano Y, Iwasaki T, Harada Y and Hatano M 2019 *Japan J. Appl. Phys.* **58** SIIB26
[79] Acosta V M *et al* 2009 *Phys. Rev.* B **80** 115202
[80] Capelli M, Heffernan A H, Ohshima T, Abe H, Jeske J, Hope A, Greentree A D and Reineck P Gibson B C 2019 *Carbon* **143** 714–9
[81] Sabella A, Spence D J and Mildren R P 2015 *IEEE J. Quantum Electron.* **51** 1–8
[82] Dréau A, Lesik M, Rondin L, Spinicelli P, Arcizet O, Roch J F and Jacques V 2011 *Phys. Rev.* B **84** 195204
[83] Levine E V, Turner M J, Kehayias P, Hart C A, Langellier N, Trubko R, Glenn D R, Fu R R and Walsworth R L 2019 *Nanophotonics* **8** 1945–73
[84] Barry J F, Turner M J, Schloss J M, Glenn D R, Song Y, Lukin M D, Park H and Walsworth R L 2016 *Proc. Natl Acad. Sci. USA* **113** 14133–8
[85] Fescenko I, Jarmola A, Savukov I, Kehayias P, Smits J, Damron J, Ristoff N, Mosavian N and Acosta V M 2020 *Phys. Rev. Res.* **2** 023394
[86] Zhang C, Shagieva F, Widmann M, Kuebler M, Vorobyov V, Kapitanova P, Isoya J and Wrachtrup J 2020 arXiv:2012.15706